$Zn_{x-1}Cu_xMn_2O_4$ Spinels; Synthesis, Structural Characterization and Electrical Evaluation

Francisco Méndez-Martínez,[1] Federico González,[2] Enrique Lima,[1] Pedro Bosch,[1] and Heriberto Pfeiffer[1,*]

[1] Instituto de Investigaciones en Materiales, Universidad Nacional Autónoma de México, Circuito Exterior, Ciudad Universitaria, Coyoacán 04510, México DF, México. Phone: +52 (55) 56224627; Fax: +52 (55) 56161371.
pfeiffer@iim.unam.mx

[2] Universidad Autónoma Metropolitana, Iztapalapa, Av. San Rafael Atlixco No. 186 Col. Vicentina, 09340 México D.F., Mexico.

Abstract. This work presents the structural characterization and electrical evaluation of $Zn_{x-1}Cu_xMn_2O_4$ spinels, which are materials presented as secondary phases into the varistor ceramic systems. Samples were analyzed by X-ray diffraction, solid-state nuclear magnetic resonance, infrared spectroscopy, scanning electron microscopy and impedance spectroscopy. Although, the addition of copper to the $ZnMn_2O_4$ spinel did not produce morphological changes, the structure and electrical behaviors changed considerably. Structurally, copper addition induced the formation of partial inverse spinels, and its addition increases significantly the electrical conductivity. Therefore, the formation of $Zn_{x-1}Cu_xMn_2O_4$ spinels, as secondary phases into the varistor materials, may compromise significantly the varistor efficiency.
Keywords*:* Ceramic, Impedance Spectroscopy, spinel, Varistor, XRD.

Resumen. En este trabajo se presenta la caracterización estructural y eléctrica de las espinelas del tipo $Zn_{x-1}Cu_xMn_2O_4$, los cuales son materiales que se pueden encontrar como fases secundarias en los cerámicos de tipo varistor. Las muestras fueron caracterizadas por difracción de rayos X, resonancia magnética nuclear de sólidos, espectroscopía infrarroja, microscopía electrónica de barrido y espectroscopía de impedancia. La adición de cobre no produce cambios morfológicos en los materiales. Sin embargo, la estructura cristalina y propiedades eléctricas si se ven considerablemente alteradas por la adición de cobre a la espinela. Estructuralmente, la adición de cobre genera la formación de espinelas parcialmente inversas y eléctricamente estos materiales se vuelven mucho más conductores. Por lo tanto, la formación de espinelas de tipo $Zn_{x-1}Cu_xMn_2O_4$, como fases secundarias en los materiales de tipo varistor, puede comprometer significativamente la eficiencia del varistor.
Palabras clave: Cerámica, espectroscopía de impedancia, espinelas, varistor, espectroscopía infrarroja.

Introduction

Due to their highly non-linear electrical properties, varistor ceramics are technologically important. This kind of ceramics may be used as reversible electrical switches. Indeed, they work as insulators or high electrical conductors depending on the current to voltage ratio [1]. Among these ceramics, zinc oxide varistors are, probably, some of the most required. They are usually produced by doping ZnO with small amounts of some other oxides. In this way, the electrical characteristics of the ZnO grain boundaries are controlled and/or modified to optimize the varistor behavior [1]. Initially, ZnO was doped with Bi or Pr [1-3]. However, in recent years, it has been shown that ZnO doped with lighter elements presents a varistor behavior as well [2, 3]. Some of the most common elements used to dope ZnO are vanadium, manganese or cobalt, among others [1-8]. However, the addition of these elements usually produces the formation of secondary phases [1, 5, 9, 10].

The so called secondary phases are mostly composed by spinel-structure materials. The general formula of spinels, AB_2O_4, embraces a wide variety of A and B atoms [11]. The valences of A and B can be 2 and 3 as in $ZnMn_2O_4$, where Zn^{2+} is located in tetrahedral sites and Mn^{3+} in octahedral sites. This kind of elemental distribution is known as normal spinel, the corresponding general formula is written as $A^{tet}B^{oct}_2O_4$.

However, the A and B ions may swap positions, partially or totally, producing the so called partial inverse or inverse spinels [11].

In most varistor systems, the formation of secondary phases has been shown [12]. Nevertheless, systematic studies to analyze if the presence of these so called secondary phases improves or decreases the ZnO electrical varistor behavior have not been reported. The aim of this work was to synthesize and analyze the electrical behavior of copper induced secondary phases. Specifically, this work was devoted to the $ZnMn_2O_4$ spinel and the solid solutions obtained with copper ($Zn_{1-x}Cu_xMn_2O_4$).

Results and discussion

Structural characterization

$ZnMn_2O_4$ and $CuMn_2O_4$ spinels, as well as their solid solutions ($Zn_{1-x}Cu_xMn_2O_4$), were synthesized. The XRD pattern of the synthesized $ZnMn_2O_4$ fitted very well with the corresponding JCPDS file 71-2499 (Figure 1), which corresponds to a tetragonal system. Within limits of X-ray diffraction, the obtained $ZnMn_2O_4$ did not show any impurity. If $ZnMn_2O_4$ was doped with copper to prepare $Zn_{1-x}Cu_xMn_2O_4$, up to x = 0.2, the XRD pattern remained unchanged, no other compound

than $ZnMn_2O_4$ could be identified. However, if the copper amount was increased to x equal 0.3 or higher values, several secondary phases became evident. Additionally, in those cases the sample crystallinity decreased significantly, as can be seen due to the variations on the peak intensities, which decreased with the copper addition. When *x* was increased between 0.4 and 0.8, another compound, $CuMn_2O_4$, could be identified (JCPDS file 84-0543), which in this case corresponds to a cubic system. If copper content was increased to 0.9, in addition to these spinel structures, Mn_2O_3 and $Cu_{0.451}Mn_{0.549}O_4$ oxides were formed. Finally, even when $x = 1$, *i.e.* $CuMn_2O_4$ composition, no pure $CuMn_2O_4$ was obtained as Mn_2O_3 and $Cu_{0.451}Mn_{0.549}O_4$ were also produced.

These results show that copper solubility into zinc-manganese spinel is 0.2, $Zn_{0.8}Cu_{0.2}Mn_2O_4$. On the other hand, when copper became the main M^{2+} cation, a different manganese phase was formed 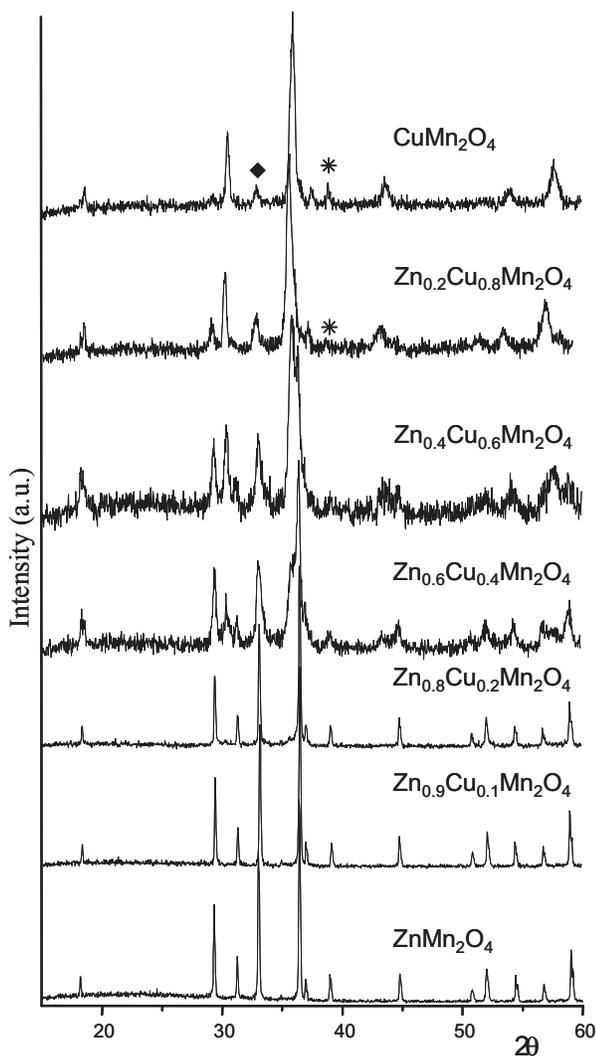Mn_2O_3. This behavior strongly suggests that the spinels are inverse spinels, with Cu^{2+} and Zn^{2+} occupying A^{2+} and B^{3+} positions. Such behavior may be explained in terms of the $CuMn_2O_4$ and $ZnMn_2O_4$ ionic radii. Copper ionic radius (0.71 Å) is slightly smaller than that of zinc (0.74 Å). This should favor the solid solution synthesis [13].

Further analyses were only performed on the pure $ZnMn_2O_4$ sample, as well its solid-solutions ($Zn_{0.9}Cu_{0.1}Mn_2O_4$ and $Zn_{0.8}Cu_{0.2}Mn_2O_4$), so FTIR and solid state NMR experiments were performed on these samples. FTIR spectra are shown in figure 2. Four absorption bands in the window 850-400 cm^{-1} were observed. The first band appeared at around 475-490 cm^{-1} and corresponded to the Zn-O vibrations [14]. As expected, this band did not present any shift, only its intensity seemed to slightly decrease as a function of the copper addition. This result indicates that Zn^{2+} cations only occupy one structural position, the A^{2+} position into the spinel structure. Cu-O band, at 610-630 cm^{-1}, is not evident, as it is partially overlapped with two different Mn-O bands. Still, the band seems to be shifted to higher wavenumbers, from 616 to 630 cm^{-1}. It seems, therefore, that copper-oxygen bonds become stronger, i.e., copper ions are not located at the same crystallographic positions in each sample. Finally, Mn-O bonds present two different band vibrations at 580-595 cm^{-1} and 670-680 cm^{-1}. Although this analysis cannot be conclusive, the Cu-O band behaviour suggests that copper atoms may be diffusing into the spinel structure towards a partial inverse spinel. This proposition is in agreement with the XRD results.

Changes in the environment of copper were shown by ^{65}Cu NMR. It seems that two chemical environments of copper are possible. Actually, both NMR signals could be related to copper sites with different coordination. This was expected because in a spinel structure copper ions can be tetrahedrally
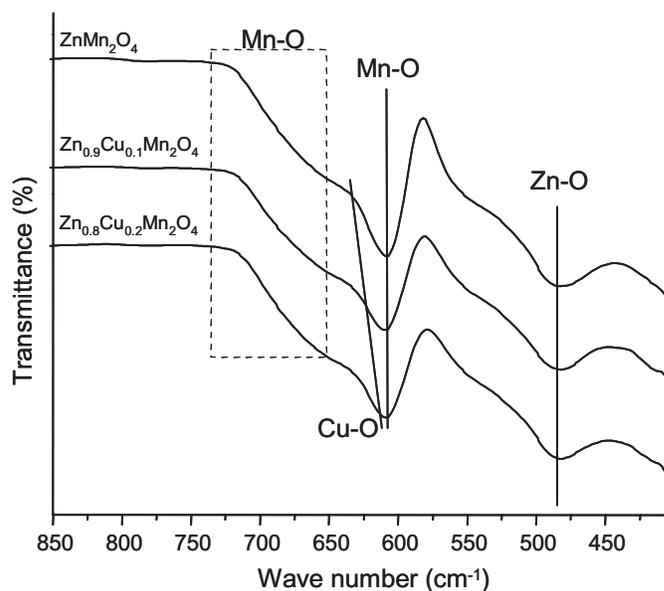

Fig. 1. X-ray diffraction patterns of the $Zn_{x-1}Cu_xMn_2O_4$ samples with tetragonal (zinc) and cubic (copper) systems. Only the Mn_2O_3 (∗) and $Cu_{0.451}Mn_{0.549}O_4$ (♦) phases were labeled.

Fig. 2. FTIR spectra of the $ZnMn_2O_4$ sample and its copper solid solutions ($Zn_{x-1}Cu_xMn_2O_4$, where $x = 0.1$ or 0.2).

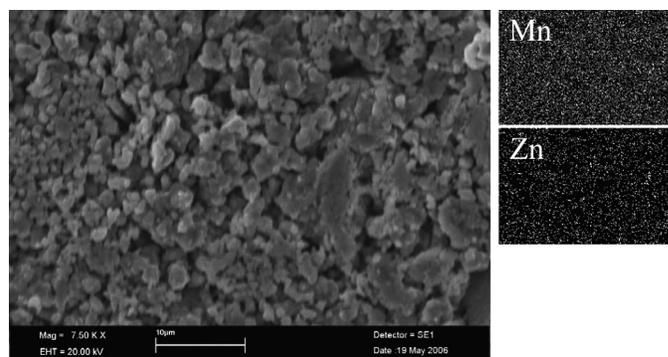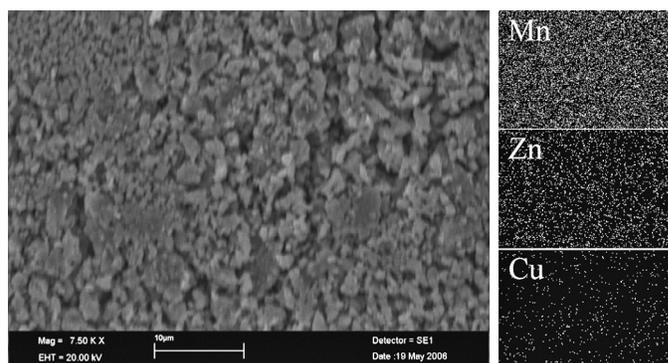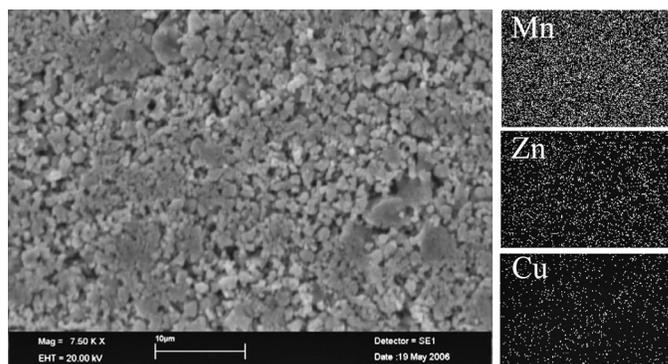**Table 1.** Integrated relative intensities of the tetrahedral/octahedral intensities measured from the NMR data.

Sample	Tetrahedral/Octahedral intensities
$ZnMn_2O_4$	0.78
$Zn_{0.9}Cu_{0.1}Mn_2O_4$	0.84
$Zn_{0.8}Cu_{0.2}Mn_2O_4$	0.90

as well as octahedrally coordinated, signals at 130 ppm and −120 ppm, respectively. From NMR results it is suggested, roughly, that population of copper in two sites is a function of the copper content. NMR data summarized on Table 1 reveal only two quadrupolar line-shapes with different integrated intensities confirming the existence of two types of site with disproportionate populations. It seems that zinc occupied tetrahedral positions, then at low copper concentration octahedral positions are preferred, and afterwards the tendency is to occupy in the same way both tetrahedral and octahedral sites.

Morphological characterization

Again, the $ZnMn_2O_4$ and the copper solid solutions ($Zn_{0.9}Cu_{0.1}Mn_2O_4$ and $Zn_{0.8}Cu_{0.2}Mn_2O_4$) samples were selected to be pelletized and sintered. Figure 3 compares the micrograph and the mapping analysis of $ZnMn_2O_4$. The pellet surface did not seem to be highly dense, and the particle size distribution was significantly broad, 1.5 to 10 μm, due to an irregular growth of the particles. Mapping and EDS analyses agreed with all the previous results, as it could be expected. While zinc and manganese mapping analyses showed a highly homogeneous elemental distribution, EDS measurements indicated a Mn/Zn molar ratio of 1.95 (Mn = 66 % and Zn = 34 %) fitting very well with the theoretical value of Mn/Zn = 2.0.

Figure 4 shows a secondary electron image and copper, zinc and manganese mapping analyses of the $Zn_{0.9}Cu_{0.1}Mn_2O_4$ pellet surface. In this case, although the sample did not seem to be highly dense, as the previous one, the particle size is more homogeneous as it only varied between 1 and 5 μm. Therefore, copper inhibited the growth of large spinel particles. Additionally, mapping and EDS analyses confirmed that copper was homogeneously distributed in the spinel; experimental elemental concentration fitted well with the nominal one, Cu = 3.4 at%; Zn = 29.9 at%; Mn = 66.7 at%. Results obtained with the sample $Zn_{0.8}Cu_{0.2}Mn_2O_4$ were similar, figure 5. The pellet was, again, not very dense and particle size interval was 1 to 5 μm. Mapping did not show any kind of element segregation, and the EDS reproduced, again, the nominal composition: Cu = 8.0 at%; Zn = 28.2 at%; Mn = 63.8 at%. The morphological characterization showed that spinel and solid solutions pellets were not highly dense and that copper addition slightly improved the homogeneity of particle size. Additionally, the

Fig. 3. SEM image and elemental mapping of $ZnMn_2O_4$ surface pellet.

Fig. 4. SEM image and elemental mapping of $Zn_{0.9}Cu_{0.1}Mn_2O_4$ surface pellet.

Fig. 5. SEM image and elemental mapping of $Zn_{0.8}Cu_{0.2}Mn_2O_4$ surface pellet.

three elements were homogeneously distributed and their experimental concentrations were the nominal ones.

Electrical tests

Impedance measurements were made on the $ZnMn_2O_4$ and $Zn_{0.8}Cu_{0.2}Mn_2O_4$ samples in air. The spectra were obtained at different temperatures between room temperature (26 °C) and 167 °C. Typical impedance complex plane plots, Z′′ vs. Z′ are shown in Figures 6 -A and −B. At room temperature,

ZnMn$_2$O$_4$ presented a total resistance of about 12 MΩ, (Figure 6 (A)), but it was decreasing as a function of the temperature up to 50 KΩ at 167 °C. In both cases, values were estimated from the intersection of the arc with the Z′ axis at low frequency. The impedance complex plane plots showed a single arc. In the ideal scenario the arc is a semicircle, indicative of a single parallel RC component. The impedance complex plane plots showed in Fig 6, depart of the ideal behaviour, however its shape is related to the presence of a very resistive element, which dominates the overall sample resistance at all temperatures studied. Therefore, a 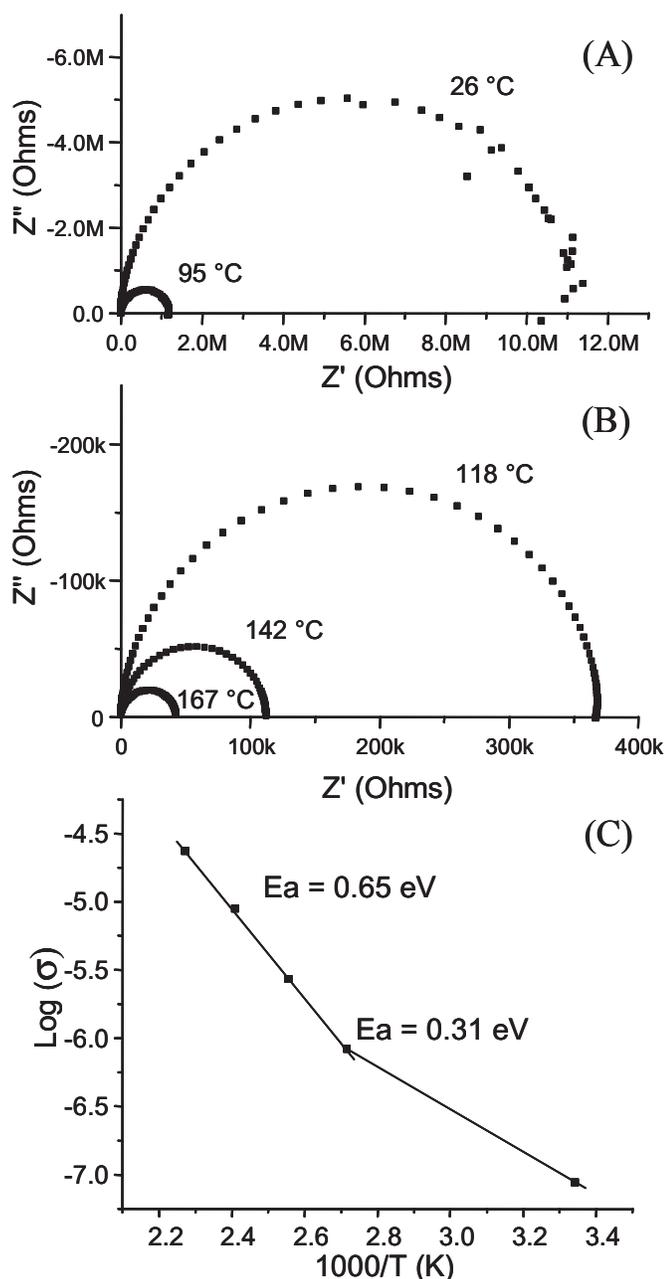single parallel RC component was used as an approximation to fit these data, with R representing the total resistance of the sample. Furthermore, the conductivity (σ) behaves like R^{-1}; thus, values of R as a function of temperature are summarized in Arrhenius (σ = e$^{-Ea/kT}$) conductivity format (Figure 6-C). It can be seen that between 26 and 95 °C sample possesses low conductivities. Then, at higher temperatures than 95 °C, the conductivity increases. Something else has to be pointed out, the activation energy, at low temperatures, is small, 0.31 eV. However, thinking on a varistor system, this low activation energy is the potential energy necessary to propitiate the electron flux, giving place to the typical insulator-conductor transition in varistor ceramics.

Finally, Figure 7 shows the impedance spectra of the Zn$_{0.8}$Cu$_{0.2}$Mn$_2$O$_4$ pellet. As can be seen the copper addition strongly modify the electrical behavior. In this sample, the resistance is three orders of magnitude smaller than those observed on the copper free sample. For example at room temperature, while ZnMn$_2$O$_4$ presented a resistance of about 12 MΩ (ρ = 4.7 × 10^5 Ωm), Zn$_{0.8}$Cu$_{0.2}$Mn$_2$O$_4$ only presented a resistance of 10.5 kΩ (ρ = 4.1 × 10^2 Ωm). For the solid solution, the spectra only could be measured at T = 95 °C, and in this case, it was not possible to obtain complete arcs in the impedance complex plane plots for all temperatures, due to the equipment frequenty limitations, and to the electrical behavior of the samples.

Conclusions

The synthesis, characterization and electrical evaluation of ZnMn$_2$O$_4$ and the copper solid solutions Zn$_{1-x}$Cu$_x$Mn$_2$O$_4$ were studied. Results indicate that copper solubility limit into the ZnMn$_2$O$_4$ spinel is 0.2, Zn$_{0.8}$Cu$_{0.2}$Mn$_2$O$_4$. Further addition of copper produced the formation of different phases. Results suggest that copper addition favors the formation of an inverse spinel, where most copper atoms are first located into tetrahedral and octahedral positions and, at high contents, occupy more octahedral positions. The morphological characterization (SEM) showed that copper is homogeneously distributed in the zinc spinel, at a micrometric scale. Moreover, copper addition
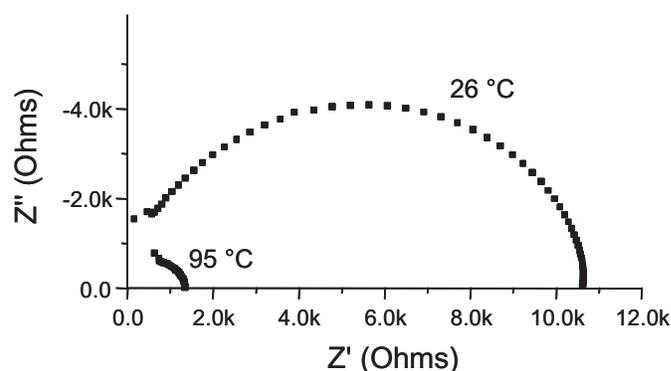

Fig. 6. Impedance curves (A) and (B) as well as the Arrhenius conductivity curve (C) of the ZnMn$_2$O$_4$ pellet.

Fig. 7. Impedance curve of Zn$_{0.8}$Cu$_{0.2}$Mn$_2$O$_4$ pellet.

inhibits particle growth. While the $ZnMn_2O_4$ sample presented a particle size of 15 μm, the copper solid solutions decreased their size up to 5 μm.

Finally, the electrical tests clearly showed that copper addition increases significantly electrical conductivity. Therefore, when this material is produced as a secondary phase during the varistor synthesis, the efficiency of the varistor may be highly compromised. The high conductivity of this material may produce a high current leak with the corresponding electron flux that has to be avoided in varistor ceramics.

Experimental section

Zinc and copper spinels, as well as their solid solutions, were synthesized, using a pyrolysis procedure. The reagents were manganese nitrate ($Mn(NO_3)_2 \times XH_2O$, Aldrich), zinc nitrate ($Zn(NO_3)_2 \times 6H_2O$, Aldrich) and copper nitrate ($Cu(NO_3)_2 \times 2.5H_2O$, Aldrich). The hydration degree of the different nitrates was evaluated by thermogravimetric analysis. In each case, reagents were dissolved stoichiometrically in water and, then, the two or three solutions were mixed dropwise. This solution was stirred for 20 min and then heated up to 60-70 °C till it dried. The powders were pulverized and fired at 900 °C for 14 hours. In the solid solutions $Zn_{1-x}Cu_xMn_2O_4$ the x value was varied from 0.1 to 0.9.

All the synthesized spinels were characterized by X-ray diffraction (XRD), scanning electron microscopy (SEM), infrared (FTIR) and solid state nuclear magnetic resonance (NMR) spectroscopies. They were tested electrically by impedance spectroscopy. The XRD patterns were obtained with a BRUKER axs D8 diffractometer coupled to a Cu anode X-ray tube. The $k_{\alpha 1}$ wavelength was selected with a diffracted beam monochromator, and the compounds were identified conventionally using the database of the Joint Committee for Powder Diffraction Standards (JCPDS). FTIR spectra were recorded in a Perkin–Elmer equipment, model Spectrum GX FTIR, from 4000 to 400 cm^{-1}. The powders were pelletized with KBr to perform these analyses. ^{65}Cu MAS NMR spectra were acquired on a Bruker Avance 2 spectrometer at 85.2 MHz, with a standard 4-mm Bruker MAS probe. At least 20 000 scans were accumulated for each spectrum. Chemical shifts, reported in parts per million, are relative to a 1 N aqueous solution of copper nitrate. SEM (Stereoscan 440, Leica-Cambridge) was used to determine the size and morphology of the particles, as

well as to determine the elemental composition (EDS) and the elemental distribution (mapping). Finally temperature dependent dielectric measurements were performed using an Agilent 4294A impedance analyzer. Data being collected over the frequency range of 100 to 10 MHz. The rms applied voltage was 0.5 V. Previously, samples were pelletized (10 mm in diameter and 2 mm in thickness) and silver painted. The electrodes of the samples were attached to the Pt leads of a conductivity cell which was placed inside a Barnstead Thermoline 47900 furnace whose temperature was controlled and measured to ±3°C. All measurements were performed between room temperature and 167 °C, in intervals of 20 °C.

References

1 Clarke, D. R. *J. Am. Ceram. Soc.* **1999**, *82*, 485–502.
2 Kuo, C. T.; Chen, C. S.; Lin, I. N. *J. Am. Ceram. Soc.* **1998**, *81*, 2942–2948.
3 Kuo, C. T.; Chen, C. S.; Lin, I. N. *J. Am. Ceram. Soc.* **1998**, *81*, 2949–2956.
4 Han, J.; Mantas, P. Q.; Senos, A. M. R. *J. Eur. Ceram. Soc.* **2002**, *22*, 49–59.
5 Pfeiffer, H.; Knowles, K. M. *J. Eur. Ceram. Soc.* **2004**, 24, 1199–1203.
6 Méndez-Martínez, F.; Venegas, M. J.; Pfeiffer, H. *Int. J. Appl. Ceram. Technol.* **2007**, *4*, 564–570.
7 Hng, H. H.; Knowles, K. M. *J. Am. Ceram. Soc.* **2000**, 83, 2455–2462.
8 Hng, H. H.; Chan, P. L., *Mater. Chem. Phys.* **2002**, *75*, 61–66.
9 Brown, J. J.; Hummel, F. A. *Trans. Br. Ceram. Soc.* **1965**, *64*, 419–437.
10 Gopal, R.; Calvo, C. *Can. J. Chem.* **1973**, 51, 1004–1009.
11 West, A. R. *Solid State Chemistry and its Application*, J. Wiley & Sons, New York, **1990**.
12 Magri, R.; Zunger, A. *Phys. Rev. B*, **2001**, *64*, 1–5.
13 Shannon, R.D. *Acta Cryst. A* **1976**, *32*, 751–767.
14 Nakamoto, K. *Infrared and Raman Spectra of Inorganic and Coordination Compounds, Part I: Theory and Applications in Inorganic Chemistry*, J. Wiley & Sons, New York, **1997**.